Superconducting properties of $Y_xLu_{1-x}Ni_2B_2C$ and $La_3Ni_2B_2N_{3-\delta}$: A comparison between experiment and Eliashberg theory

S. Manalo, H. Michor, M. El-Hagary, and G. Hilscher
Institut für Experimentalphysik, Technische Universität Wien, Wiedner Hauptstraße 8-10, A-1040 Wien, Austria

E. Schachinger
Institut für Theoretische Physik, Technische Universität Graz, Petersgasse 16, A-8010 Graz, Austria
(Received 18 November 1999; revised manuscript received 26 June 2000; published 14 February 2001)

Specific heat and resistivity measurements were performed on polycrystalline samples of the solid-solution $Y_xLu_{1-x}Ni_2B_2C$ in order to determine thermodynamic properties such as the specific-heat difference ΔC, the thermodynamic critical field $H_c(T)$, as well as the upper critical field $H_{c2}(T)$. These properties were analyzed within the Eliashberg theory including anisotropy effects, yielding electron-phonon coupling anisotropy parameters $\langle a_{\mathbf{k}}^2 \rangle$ ranging between 0.02 and 0.03 for the whole series, and Fermi velocity anisotropy parameters of $\langle b_{\mathbf{k}}^2 \rangle = 0.245-0.3$. Excellent agreement between theory and experiment was achieved for these parameters, the Sommerfeld constant γ and model phonon spectra determined from specific heat measurements. An analysis of the previously investigated boronitride $La_3Ni_2B_2N_{3-\delta}$ for comparison revealed the electron-phonon anisotropy to be of great significance in describing its thermodynamic properties and the calculations yielded $\langle a_{\mathbf{k}}^2 \rangle \simeq 0.08$ and $\langle b_{\mathbf{k}}^2 \rangle \simeq 0.245$. The T_c behavior within the series $Y_xLu_{1-x}Ni_2B_2C$ is discussed in terms of the density of states at the Fermi level $N(0)$.

DOI: 10.1103/PhysRevB.63.104508 PACS number(s): 74.25.Bt, 74.70.Dd, 74.62.Yb, 74.20.−z

I. INTRODUCTION

The transition-metal borocarbide superconductors RNi_2B_2C with transition temperatures comparable to those of the A-15 compounds (e.g., $R=$Lu with $T_c \simeq 16.5$ K, Nb_3Ge with $T_c \simeq 23$ K) are a subject of broad interest for research on intermetallic superconductors. Siegrist *et al.*[1] reported the crystal structure of the RNi_2B_2C superconductors to be a filled version of the $ThCr_2Si_2$-type structure stabilized by the incorporation of carbon, where Ni_2B_2 layers are separated by RC layers. In the related compound $La_3Ni_2B_2N_{3-\delta}$, three LaN planes separate the Ni_2B_2 layers. Despite of the layered structure reminiscent of the cuprate superconductors, the electronic structure of the single RC-layer borocarbides as well as the triple LaN-layer boronitride is three dimensional.[2,3] Nickel-site substitutions on both the borocarbides and the boronitride revealed similar electronic properties of the bands related to the $3d$ electrons.[4]

At a first glance, the thermodynamic properties of $La_3Ni_2B_2N_{3-\delta}$ seem to be close to the weak coupling BCS predictions,[5] but standard single-band BCS theory cannot explain the pronounced upward curvature of the upper critical field $H_{c2}(T)$ close to T_c. If applied to the borocarbides, it fails to describe both the thermodynamic properties and the upper critical field obtained from experiment. Shulga *et al.*[6] analyzed the upper critical field $H_{c2}(T)$ of $LuNi_2B_2C$ and YNi_2B_2C in terms of the Eliashberg-theory using an isotropic two-band model. An isotropic single band model cannot reproduce the positive curvature near T_c apparently, because of the dominant role of anisotropy effects in this system. Recently, Dugdale *et al.*[7] presented an experimental investigation on the Fermi surface of $LuNi_2B_2C$, revealing that it consists of three sheets.

Freudenberger *et al.*[8] studied the solid solution $Y_xLu_{1-x}Ni_2B_2C$ and showed, that T_c exhibits a minimum at about $x \simeq 0.5$ with a T_c depression of about 1 K. They pointed out, that this feature cannot be described alone by disorder effects with the residual resistivity ratio as a measure, and tentatively supposed the electron phonon coupling strength λ to be the origin of this behavior.

We present in this paper investigations of the thermodynamic properties and of the upper critical field $H_{c2}(T)$ of the series $Y_xLu_{1-x}Ni_2B_2C$ and the boronitride $La_3Ni_2B_2N_{3-\delta}$. The critical temperature, the specific heat, and the temperature dependence of the upper critical magnetic field were measured for all samples of the series $Y_xLu_{1-x}Ni_2B_2C$ and the results, including previous measurements of $La_3Ni_2B_2N_{3-\delta}$ (Ref. 5), were analyzed using an anisotropic model of the s-wave Eliashberg formalism. Considering the change in mass from Y to Lu in the series and different lattice properties of both systems, we used model phonon spectra calculated from the phonon contribution to the specific heat and found these to be sufficient in describing both the thermodynamic properties and the upper critical field of $La_3Ni_2B_2N_{3-\delta}$ and $Y_xLu_{1-x}Ni_2B_2C$. An analysis of the coupling strength and electronic density of states in $Y_xLu_{1-x}Ni_2B_2C$ gives an insight on the origin of the dip in $T_c(x)$. Section II presents details of sample preparation and measuring techniques and Sec. III shows the theoretical background used for the analysis. In Sec. IV, an analysis of the experimental data in terms of the anisotropic Eliashberg theory is discussed and possibilities for the T_c reduction are presented. Conclusions are drawn in Sec. V.

II. EXPERIMENTAL

Polycrystalline samples of $Y_xLu_{1-x}Ni_2B_2C$ were synthesized on a water-cooled copper grove by high frequency in-

duction melting under argon atmosphere. The starting materials are rare earth ingots (R=Y, Lu) (Strem chemicals, USA: 99.9%), Ni ingots (Strem chemicals, USA: 99.9%), crystalline boron (Starck, Germany: 99.5%), and carbon ingots (Starck, Germany: 99.99%). A good homogeneity was obtained by performing the following three steps of sample preparation. (i) Nickel and boron were melted two times. (ii) Rare-earth and carbon ingots were alloyed together while compensating the carbon loss (1–2 %) during the remelting stage. (iii) The two precursor alloys NiB and RC were melted together. The buttons were broken and remelted for at least 12 times, and finally annealed at 1020 °C for at least one week in evacuated quartz tubes. The phase purity of the samples was checked at room temperature by applying x-ray diffraction (XRD) in a Guinier-Huber camera using germanium as an internal standard. The x-ray photographs of the samples, indexed on the basis of the tetragonal crystal structure of $LuNi_2B_2C$ (space group $I4/mmm$), show that the samples of the solid solution $Y_xLu_{1-x}Ni_2B_2C$ are almost single phase with traces of $Y_{1-x}Lu_xB_2C_2$ and $Y_{1-x}Lu_xNi_4B$. According to the x-ray line intensities and optical micrograph investigations the total amount of these secondary phases is about 2–5 % in all samples investigated.

Specific heat measurements in the temperature range 1.5–160 K and magnetic fields up to 9 T were carried out on 1–2 g samples employing a quasiadiabatic step-heating technique. The sample holder consists of a thin sapphire disc ($m \sim 0.2$ g) with a strain gauge heater and a CERNOX temperature sensor. The field calibration of the latter has been performed against two GaAlAs resistivity thermometers and a capacitive $SrTiO_3$ sensor. Four point resistivity measurements were performed in fields up to 9 T in order to determine $H_{c2}(T)$ by means of a midpoint criterion. The transition widths according to a 10 and 90 % criterion are indicated by error bars in the figures containing the upper critical field obtained from the experiment.

The characterization of the polycrystalline $Y_xLu_{1-x}Ni_2B_2C$ samples with respect to their residual resistance ρ_0 and the room temperature residual resistance ratio (RRR) [$\equiv \rho(300\ \mathrm{K})/\rho(17\ \mathrm{K})$] turned out to be rather problematic, because our well annealed samples are rather brittle and partly textured. Thus, we had difficulties to obtain reproducible and reliable RRR values ranging between 10 and 43 (RRR$\simeq$10 for x=0.5 and 0.8, RRR=12 for YNi_2B_2C, 16 for x=0.1 and 43 for $LuNi_2B_2C$). The RRR value of 43 for $LuNi_2B_2C$ is twice as large as typical single crystal values (see, e.g., Ref. 9). For YNi_2B_2C, however, we got a much lower value of just 12 although its thermodynamic mean transition temperature T_c=15.56 K (see below) is even slightly higher than T_c=15.4 K of a high quality YNi_2B_2C single crystal[10] with RRR=37. The upper critical fields $H_{c2}(T)$ of these YNi_2B_2C specimens match to each other despite of the different RRR values (compare Fig. 11 of this work with Fig. 4 of Ref. 10). In the latter paper Nohara *et al.*[10] reported that the Sommerfeld value γ of clean limit YNi_2B_2C and $LuNi_2B_2C$ exhibits a $\sqrt{H}$ dependence which changes to a linear relation $\gamma \propto H$ in the dirty limit. We note, that we found an approximate $\gamma \propto \sqrt{H}$ dependence in all our samples including $La_3Ni_2B_2N_{3-\delta}$, although the RRR shown in Ref. 5 is only about 3, similar to the ''dirty'' $Y(Ni_{0.8}Pt_{0.2})_2B_2C$ for which $\gamma \propto H$ was reported. It is obvious that the grain boundaries of the polycrystalline samples strongly reduce the RRR value especially in $La_3Ni_2B_2N_{3-\delta}$. Further arguments for the extrinsic origin of the large residual resistance ρ_0 of $La_3Ni_2B_2N_{3-\delta}$ will be given in context with analysis of the experimental data in terms of the anisotropic Eliashberg theory (see Sec. VI E).

III. THEORETICAL BACKGROUND

Anisotropy effects have to be considered in the description of the experimental results for $H_{c2}(T)$ in order to obtain a satisfactory agreement between theory and experiment. Daams and Carbotte[11] applied the separable model introduced by Markovitz and Kadanoff[12] to describe an anisotropic electron-phonon interaction spectral function within Eliashberg theory

$$[\alpha^2F(\omega)]_{\mathbf{k},\mathbf{k}'} = (1+a_{\mathbf{k}})\alpha^2F(\omega)(1+a_{\mathbf{k}'}), \tag{1}$$

where $\mathbf{k}$ and $\mathbf{k}'$ are the incoming and outgoing quasiparticle momentum vectors in the electron-phonon scattering process and $a_{\mathbf{k}}$ is an anisotropy function describing the deviation of the anisotropic spectral function, $[\alpha^2F(\omega)]_{\mathbf{k},\mathbf{k}'}$, from the isotropic one, $\alpha^2F(\omega)$, in the direction of $\mathbf{k}$. It has the important feature that its Fermi surface average $\langle a_{\mathbf{k}} \rangle = 0$ and as anisotropy effects are rather small it is sufficient to keep only the mean-square anisotropy $\langle a_{\mathbf{k}}^2 \rangle$ as the important anisotropy parameter.

The theory of $H_{c2}(T)$ for anisotropic polycrystalline superconductors in a separable model scheme was developed by Prohammer and Schachinger.[13] It employs the separable ansatz for the anisotropy of the electron-phonon interaction and the ansatz

$$v_{F,\mathbf{k}} = (1+b_{\mathbf{k}})\langle v_F \rangle, \tag{2}$$

which describes the anisotropy of the Fermi velocity; $b_{\mathbf{k}}$ is an anisotropy function defined the same way as $a_{\mathbf{k}}$. The upper critical field is then described by the set of equations (27)–(30) in Ref. 14 and thermodynamic properties of the borocarbides were calculated using Eqs. (33)–(37) of Ref. 14. N-band models have been extensively studied as a tool to describe anisotropic features of superconductors. Shulga *et al.*[6] applied the two-band model H_{c2} equations[13] to their experimental results and were able to describe the experimental data with the corresponding equations. Thus, the separable model employed in this work can be described in its simplest form by a Fermi surface split into two half spheres of equal weight

$$P(a) = \delta(-a)/2 + \delta(a)/2, \tag{3}$$

with radii $r \pm a$, if r is the radius of the equivalent isotropic Fermi sphere.[15] Using the Fermi surface harmonics (FSH) notation introduced by Allen,[16] Daams[17] observed that this separable model was equivalently described by a restriction

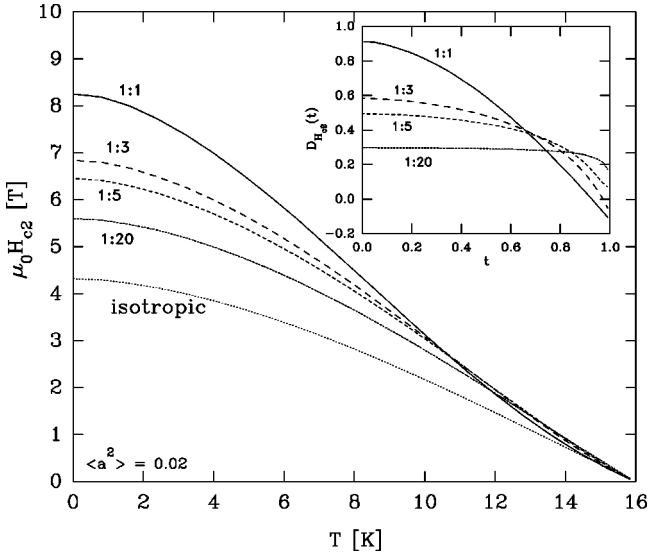

FIG. 1. Influence of different weights for the two Fermi-surface sheets on the upper critical field $H_{c2}(T)$. The numerical result in the case of equal weights (1:1) is a fit to the upper critical field of $LuNi_2B_2C$ with $\langle a^2\rangle = 0.02$, $\langle b^2\rangle = 0.25$, and $\langle v_F\rangle = 0.280\times 10^6$ m/s. $D_{H_{c2}}(t)$ is depicted in the small inset.

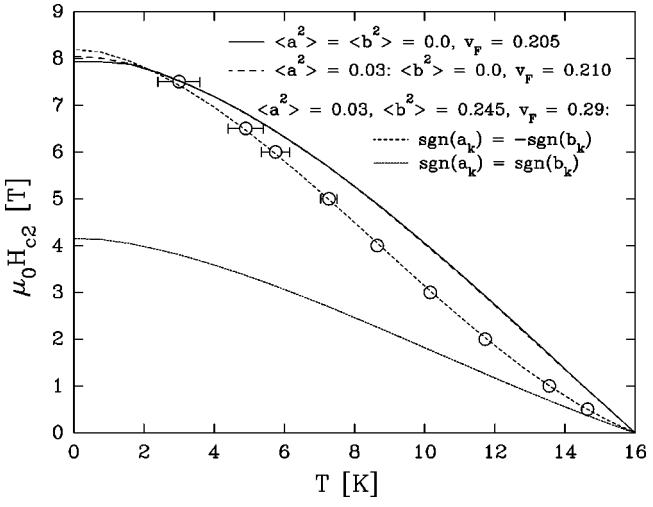

FIG. 2. Influence of different signs of $a_{\mathbf{k}}$ and $b_{\mathbf{k}}$ on the upper critical field $H_{c2}(T)$. Both Fermi-surface sheets were weighed with the same factor (1:1). The experimental result for $LuNi_2B_2C$ is labeled with open circles.

to zeroth-order FSH in each of the two subregions of the Fermi surface. According to her work, the separable model applied in our analysis corresponds to a two-band model in which the two Fermi surface regions have equal weight. It is of course also possible to define different weights for the two regions, thus changing the distribution function (3), but Daams[17] demonstrated that in the case of weak anisotropy the influence of different weights in a separable model is of negligible significance for the thermodynamics of anisotropic superconductors.

In the case of the upper critical field any deviation from the equal weight configuration causes $H_{c2}(T)$ to approach the isotropic case as is demonstrated in Fig. 1. The deviation function in the inset of Fig. 1

$$D_{H_{c2}}(T/T_c) = D_{H_{c2}}(t) = \frac{H_{c2,a}(t)}{H_{c2,i}(t)} - 1 \qquad (4)$$

demonstrates the deviation of the upper critical field of an anisotropic system $H_{c2,a}(T)$ from the upper critical field of an isotropic, equivalent system $H_{c2,i}(T)$. The numerical result for equal weights (1:1) was fitted to the upper critical field of $LuNi_2B_2C$ to fix the parameters $\langle a_{\mathbf{k}}^2\rangle$, $\langle b_{\mathbf{k}}^2\rangle$, and $\langle v_F\rangle$. The mean Fermi velocity $\langle v_F\rangle$ and its anisotropy parameter $\langle b_{\mathbf{k}}^2\rangle$ were used to fit the experimental data near T_c, and $\langle a_{\mathbf{k}}^2\rangle$ was changed to describe $H_{c2}(T)$ at lower temperatures. With these parameters, we calculated the upper critical field for different weights of the Fermi sheets $(1{:}n)$ to investigate the change in the behavior of H_{c2}. Obviously, $H_{c2,a}$ approaches $H_{c2,i}$ as one of the two sheets becomes dominant in weight and this is indicated by a flattening of $D_{H_{c2}}(t)$.

The relative signs of $a_{\mathbf{k}}$ and $b_{\mathbf{k}}$ in the same Fermi-surface sheet is also of importance to the analysis of H_{c2}. With same signs of $a_{\mathbf{k}}$ and $b_{\mathbf{k}}$ in same sheets, $H_{c2,a}(T)$ is reduced compared to $H_{c2,i}(T)$ (Fig. 2). Opposite signs within same sheets give rise to an enhancement of $H_{c2,a}$ over $H_{c2,i}$. In this case, the reduction of $H_{c2,a}(T)$ due to the influence of $\langle b_{\mathbf{k}}^2\rangle$ is compensated by the electron-phonon interaction anisotropy. Band structure calculations can give a good estimate for the weight and the relative signs of $a_{\mathbf{k}}$ and $b_{\mathbf{k}}$ in the corresponding regions of the Fermi surface. Dugdale *et al.*[7] were able to show that the Fermi surface of $LuNi_2B_2C$ consists of three sheets without giving the weights belonging to the Fermi surface regions. The third one is a small electron pocket centered at Γ, which compared to the other two sheets can be regarded to have a negligible effect on H_{c2} if considered in the theoretical calculations.

With the knowledge of the Fermi surface consisting of two dominant sheets and the shape of the experimental upper critical field favoring opposite signs of $a_{\mathbf{k}}$ and $b_{\mathbf{k}}$ within the same sheets, we used equal weights for the two Fermi surface regions and opposite signs of $a_{\mathbf{k}}$ and $b_{\mathbf{k}}$ in the following analysis. Numerical results for $H_{c2}(T)$ showed that in the case of both anisotropy functions having the same signs, the mean Fermi velocity $\langle v_F\rangle$ needed to fit the experimental data deviates significantly from the value determined from the plasma frequency.[18] The same effect on $\langle v_F\rangle$ is observed with different weights of the Fermi surface regions.

Finally, impurities are treated in Born's limit[19] which assumes the impurities to be randomly distributed and to be of dilute concentration. In such a limit impurities are characterized by a scattering rate t^+ which is proportional to the impurities' concentration. Their main effect is the smearing out of the electron-phonon interaction anisotropy resulting in a slight reduction of T_c,[12] an enhancement of H_{c2} at low temperatures, and a reduction of the high-temperature upward curvature of H_{c2} as was demonstrated by Weber *et al.*[14] for Nb.

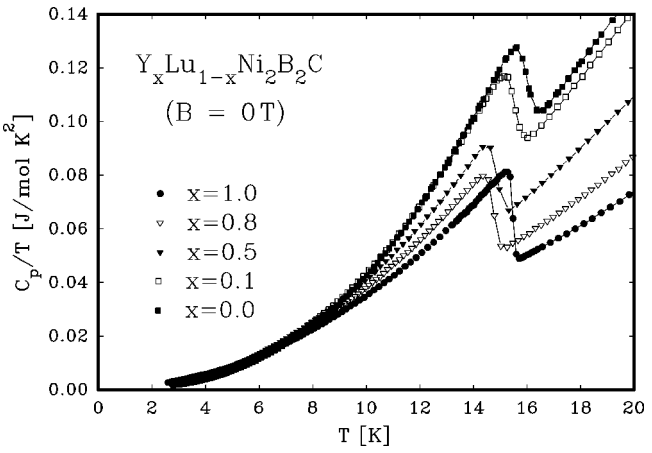

FIG. 3. C_p/T vs T plot for $Y_xLu_{1-x}Ni_2B_2C$ at zero external field.

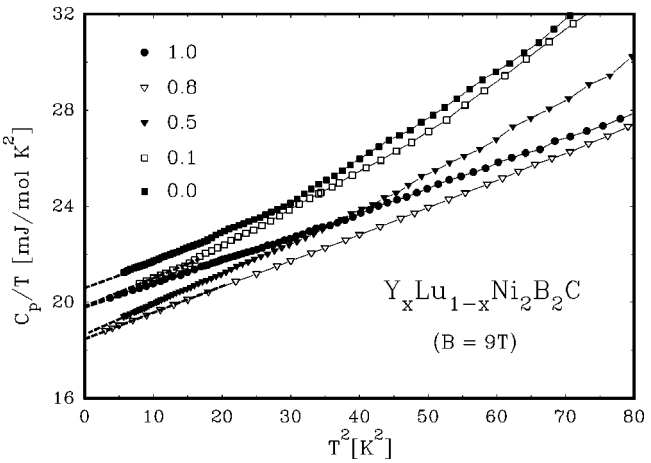

FIG. 4. C_p/T vs T^2 plot for $Y_xLu_{1-x}Ni_2B_2C$ at an external field of $B=9$ T. The straight dashed lines indicate the extrapolation of the data to $T\rightarrow 0$.

IV. RESULTS AND DISCUSSION

A. Results of the specific heat measurements

The low-temperature specific heat of $Y_xLu_{1-x}Ni_2B_2C$ with $x=0$, 0.1, 0.5, 0.8, and 1 is presented in Figs. 3–5. An external field of 9 T was applied to suppress superconductivity in order to determine the normal state heat capacity $C_n = C_e + C_{ph} = \gamma T + \beta T^3$, where γ is the Sommerfeld parameter and β is related to the low-temperature value of the Debye temperature. From the specific heat data in the normal and superconducting state (Figs. 3 and 4) we obtained the specific heat difference $\Delta C = C_s - C_n$ and used it to calculate further quantities as the thermodynamic critical field $H_c(T)$ and its deviation function $D(T)$ [Eqs. (9), (10)], which are compared to numerical results obtained with Eliashberg theory as discussed below. The extrapolation of the normal state specific heat to $T\rightarrow 0$ shown in Fig. 4 with the range of extrapolation starting at ~ 30 K^2 revealed the Sommerfeld constants of the series $Y_xLu_{1-x}Ni_2B_2C$ ranging from $\gamma = 18.5(2)$ mJ/mol K^2 for $x=0.8$ to 20.6(2) mJ/mol K^2 for $x=0$. The values for the other compounds within the series are 19.7(3) mJ/mol K^2 ($x=0.1$), 18.7(3) mJ/mol K^2 ($x=0.5$), and 19.7(2) mJ/mol K^2 ($x=1$). A comparison of the Sommerfeld constants of the border phases ($x=0,1$) with those of Ref. 20 reveals about ~ 1 mJ/mol K^2 higher values of γ in this work, with about the same T_c for $LuNi_2B_2C$ but a higher one for YNi_2B_2C compared to previous results. The difference in these properties may be explained by the homogeneity range achieved by different methods used to prepare polycrystalline materials.[21]

B. Spectral function and coupling strength

The large mass difference between Y and Lu causes a significant change of the low-energy phonon frequencies in $Y_xLu_{1-x}Ni_2B_2C$ while high energy phonon modes are hardly affected by the rare earth substitution. The latter was shown by inelastic neutron spectroscopy (INS) results on Y and $LuNi_2B_2C$ reported by Gompf *et al.*[22] Similar conclusions were also obtained from the lattice heat capacity of RNi_2B_2C (R=La, Lu, and Y) analyzed by means of a model phonon density of states (PDOS) in a previous paper.[20] The low-energy part of our model spectra were well confirmed by INS while the high-energy part is, of course, just a crude description which does not give the real details. Nevertheless, the moments of these spectra are in remarkable agreement with those calculated from the INS results. As the following discussion of superconducting properties in terms of the Eliashberg formalism requires primarily details of the low-energy PDOS we evaluated the variation of the low-energy phonon modes within the series $Y_xLu_{1-x}Ni_2B_2C$ by a similar procedure as explained in Ref. 20, i.e., by fitting the normal state specific heat measured from 2 to 160 K with a model PDOS, $F(\omega)$, which is of the form

$$F(\omega) = 3R\left(\frac{3\omega^2}{\Omega_D^3}\theta(\omega)\theta(\Omega_D-\omega)\right) + \sum_{i=0}^{3} g_i R\left(\frac{1}{\sqrt{2\pi\sigma_i^2}}\exp\left[-\frac{(\omega-\Omega_{Ei})^2}{2\sigma_i^2}\right] \times \theta(\omega-\omega_0)\theta(\Omega_{E3}-\omega)\right). \quad (5)$$

In this formula $\theta(x)$ is the well-known step function; $\omega_0 = 4.3$ meV in order to avoid a finite spectral density at zero energy; σ_i are the widths of the Gaussians and g_i are the weights of these contributions (i.e., the number of the contributing phonon branches). The Debye spectrum ($\propto\omega^2$) represents the spectral weight of the three acoustic branches and the Gaussian contributions account for the 15 optical branches. The free parameters are the Debye cutoff Ω_D and the Gaussian peak positions Ω_{E_i}, respectively. In order to fix a high-energy limit of the model spectrum, the Gaussian contribution with the highest energy (Ω_{E_3}) was cut off at the peak position and g_3 is accordingly doubled in Eq. (5). The parameters applied in Eq. (5) are summarized in Table I. The only difference with respect to the model spectra shown in Ref. 20 is the splitting up of Ω_{E_1} with $g_1=1.5$ into two parts

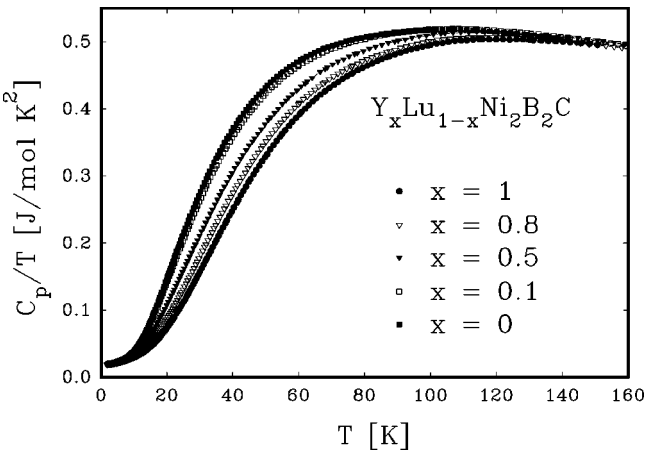

FIG. 5. Normal-state contribution to the specific heat of $Y_xLu_{1-x}Ni_2B_2C$.

Ω_{E_0} and Ω_{E_1} with $g_0=0.3$ and $g_1=1.2$, respectively, which was motivated by the shape of $F(\omega)$ obtained by INS on YNi_2B_2C (see Ref. 22). On the other hand we now fixed Ω_{E_3} to 103.4 meV (equivalent to 1300 K$\times k_B$) in order to keep the number of parameters small. Only for $Y_{0.5}Lu_{0.5}Ni_2B_2C$ we applied a slightly modified spectrum with $g_0=0.7$ and $g_1=0.8$ compared to 0.3 and 1.2 given in Table I, because of the fifty to fifty ratio of Y and Lu in this sample.

Adjusting the model spectra to the lattice heat capacity via

$$C_{ph}(T)=R\int_0^\infty d\omega F(\omega)\frac{(\omega/2T)^2}{\sinh^2(\omega/2T)}, \tag{6}$$

we obtained the model spectra shown in Fig. 6. This procedure provides a satisfactory description of the $C_P(T)$ data from 2 up to 160 K (up to 300 K for the border phases).

The phonon contribution to the specific heat yields information on $F(\omega)$ rather than on $\alpha^2F(\omega)$. Therefore, one is led to introduce an assumption on the form of the electron-phonon coupling function $\alpha^2(\omega)$. Junod *et al.*[23] suggested a function $\alpha^2(\omega)\sim\omega^s$ in a first approximation and found the exponent to be $s=-1/2$ for a large number of $A15$ compounds by comparing the experimentally determined moments of $\alpha^2F(\omega)$ with tunneling data. We calculated the thermodynamic properties of the borocarbides using $s=0$, $-1/2$, and -1, and found the exponent $s=-1/2$ to be the best choice for the theoretical analysis as in the case of the $A15$ compounds. It was impossible to describe the experimental data using $s=0$ because the theoretical deviation function $D(t)$ already lies below the experiment for an isotropic system, as a consequence of the large Gaussian contribution above the low-temperature Debye frequency Ω_D^{LT}, and is expected to get more negative for an anisotropic system. In the case of $s=-1$ the calculated deviation function is significantly larger than the experimental one and a consistent description of the thermodynamic properties and H_{c2} is impossible because of the large anisotropy parameter $\langle a_{\mathbf{k}}^2\rangle$ necessary to describe the thermodynamic properties.

TABLE I. Parameters of the model spectrum.

cont.	Ω_D	Ω_{E_0}	Ω_{E_1}	Ω_{E_2}	Ω_{E_3} (cutoff)
	free	free	free	free	103.4 meV (fixed)
σ_i (meV)		1.6	1.6	12.1	25.9
g_i	3	0.3	1.2	8.5	5

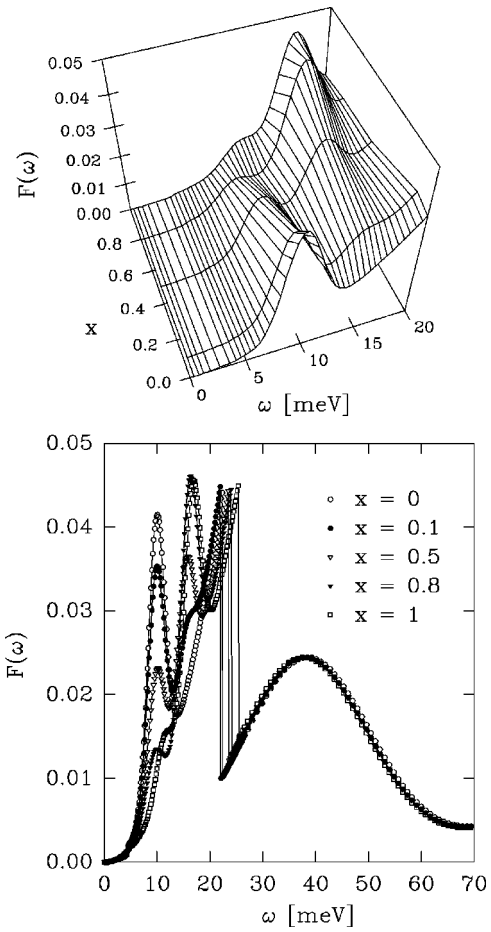

FIG. 6. Model phonon spectra obtained from the phonon contribution to the specific heat. The spectral densities $\alpha^2F(\omega)$ used in the analysis of $Y_xLu_{1-x}Ni_2B_2C$ were obtained by applying a coupling function $\alpha^2(\omega)\sim\omega^{-1/2}$ to the model PDOS. The three-dimensional plot shows the evolution of modes vs x of $F(\omega)$.

The spectra were cut off at the local minimum of the model phonon spectra at $\omega\sim68$ meV. Starting at this energy, the phonon spectra determined by Gompf *et al.*[22] using inelastic neutron-scattering techniques have a wide interval, where the PDOS is zero. The next optical contributions to $F(\omega)$ start at ~100 meV, and it is not very likely that electrons still considerably couple to phonons at these energies.

With the coupling function having the form $\alpha^2(\omega)=a\omega^{-1/2}$, the model spectra shown in Fig. 6 were weighed with a function $\omega^{-1/2}$ and were rescaled with a constant a to give the corresponding critical temperatures T_c of the samples for a fixed pseudopotential of $\mu^*=0.13$. The model spectral functions give electron-phonon interaction mass enhancement factors

TABLE II. Parameters used for the calculation of thermodynamic properties of $Y_xLu_{1-x}Ni_2B_2C$. The mass enhancement factor or electron-phonon coupling factor λ, the number of atoms in a certain volume, n_A, and the Sommerfeld constant used in the theoretical description γ_c, are compared within the series $Y_xLu_{1-x}Ni_2B_2C$.

x	T_c [K]	λ	n_A [10^{22}/cm^3]	γ_c [mJ/mol K^2]
0	16.01	1.220	9.405	19.7
0.1	15.56	1.182	9.382	18.9
0.5	14.90	1.058	9.263	18.1
0.8	14.68	1.018	9.220	18.0
1	15.45	1.017	9.175	18.6

$$\lambda = 2\int_0^\infty d\omega \frac{\alpha^2 F(\omega)}{\omega} \tag{7}$$

between 1.02 ($x=1$) and 1.22 ($x=0$). λ does not behave as the critical temperature and descends monotonically from $LuNi_2B_2C$ to YNi_2B_2C as a function of x, without showing a minimum, which indicates that it cannot account alone, if at all, for the depression of T_c within the series.

C. Thermodynamic properties and $H_{c2}(T)$

With the set of parameters given in Table II, the thermodynamic properties were calculated for all samples. The number of atoms in a volume of 1 cm^3, n_A, was calculated from lattice parameters a and c of the tetragonal structure. The Sommerfeld constants obtained from the experiment $\gamma_{\rm exp}$, are slightly greater than the theoretical values γ_c, needed to fit the experimental results for the thermodynamic critical field $H_c(T)$. The latter is calculated from the experimental data by integrating the difference between the zero-field and 9 T measurement, i.e., any normal state contribution to the zero-field heat capacity cancels out in $\Delta C = C_s - C_n \hat{=} C(0\ \mathrm{T}) - C(9\ \mathrm{T})$ which is used in the analysis below. Nevertheless, a normal state contribution, which is eliminated in ΔC, will strongly influence the experimental result for the temperature dependence of the electronic specific heat in the superconducting state $C_{eS}(T)$, obtained by subtracting the phonon contribution from the zero-field data. We note, that the γ value due to a small amount of impurity phase obtained by extrapolating the zero field data in a C/T vs T^2 plot to $T\rightarrow 0$ yields, e.g., for YNi_2B_2C $\gamma_{\rm imp} \simeq 0.4(2)$ mJ/mol K^2 which is significantly smaller than $\gamma_{\rm exp} - \gamma_c \sim 1.1$ mJ/mol K^2. For all other samples, $\gamma_{\rm imp}$ is found to be even closer to zero, but $\gamma_{\rm exp} - \gamma_c$ is still about 1 mJ/mol K^2 (see Fig. 7). Thus, the average difference of about 5% may be attributed to an intrinsic effect, namely, to the contribution of the small electron pocket, for which de Haas–van Alphen measurements performed by Terashima *et al.*[24] revealed the superconducting gap to be much smaller than on other parts of the Fermi surface. For a further discussion of the temperature dependence of $C_{eS}(T)$ see below (Sec. IV F).

In the description of the thermodynamics and the upper critical field of $Y_xLu_{1-x}Ni_2B_2C$ the model spectra of Fig. 6 were used in the numerical solution of the Eliashberg equations in the clean limit (impurity scattering rate $t^+ = 0$). This is of course only a rough approximation and the corresponding scattering rate t^+ should be determined from a T_c reduction with increasing concentrations of Born limit momentum scattering impurities.[14] As it was not possible to perform this type of experiment with the present samples we investigated the influence of impurity concentration theoretically and realized that in order to stay within the constraints of the known experimental data t^+ had to be rather small and therefore we regarded the clean limit to be an acceptable approximation. As the coherence length is rather short in these materials the clean limit is always a good approximation. The results of our theoretical study of different spectral functions $\alpha^2F(\omega)$ and of the influence of impurities on the thermodynamics as well as on H_{c2} will be the topic of a separate, forthcoming publication.

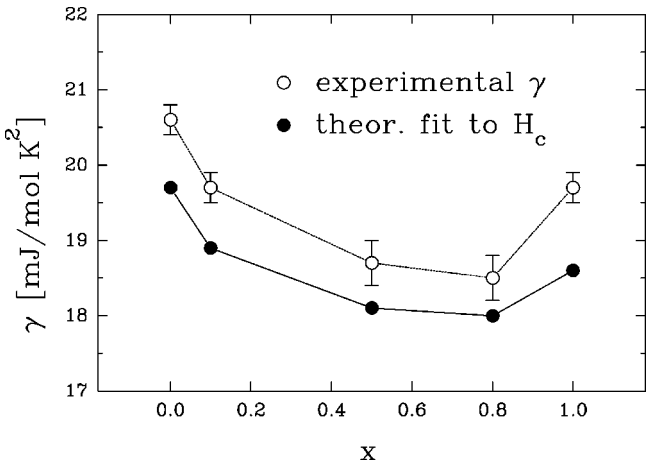

FIG. 7. Sommerfeld constants used in the theoretical description compared to those obtained from specific heat measurements.

Figure 8 depicts the comparison between experimental results and theoretical predictions for $LuNi_2B_2C$. The top frame shows the specific heat difference between superconducting and normal state $\Delta C(T) = C_s(T) - C_n(T)$. Theoretical calculations were done for an isotropic ($\langle a_{\mathbf{k}}^2 \rangle = 0$) and an anisotropic case ($\langle a_{\mathbf{k}}^2 \rangle = 0.03$), and results with anisotropy parameters between these values lie in between the numerical results of Figs. 8(a)–8(c). Considering impurity scattering would bring the results of an anisotropic calculation closer to the isotropic case.

The thermodynamic critical field $H_c(T)$ is calculated from the free energy difference ΔF

$$H_c(T) = \sqrt{2\Delta F/\mu_0}, \tag{8}$$

and the specific heat difference ΔC is related to ΔF through

$$\Delta C(T) = -T\frac{\partial^2 \Delta F(T)}{\partial T^2}. \tag{9}$$

Strong coupling and anisotropy effects can be observed in the deviation function of the thermodynamic critical field

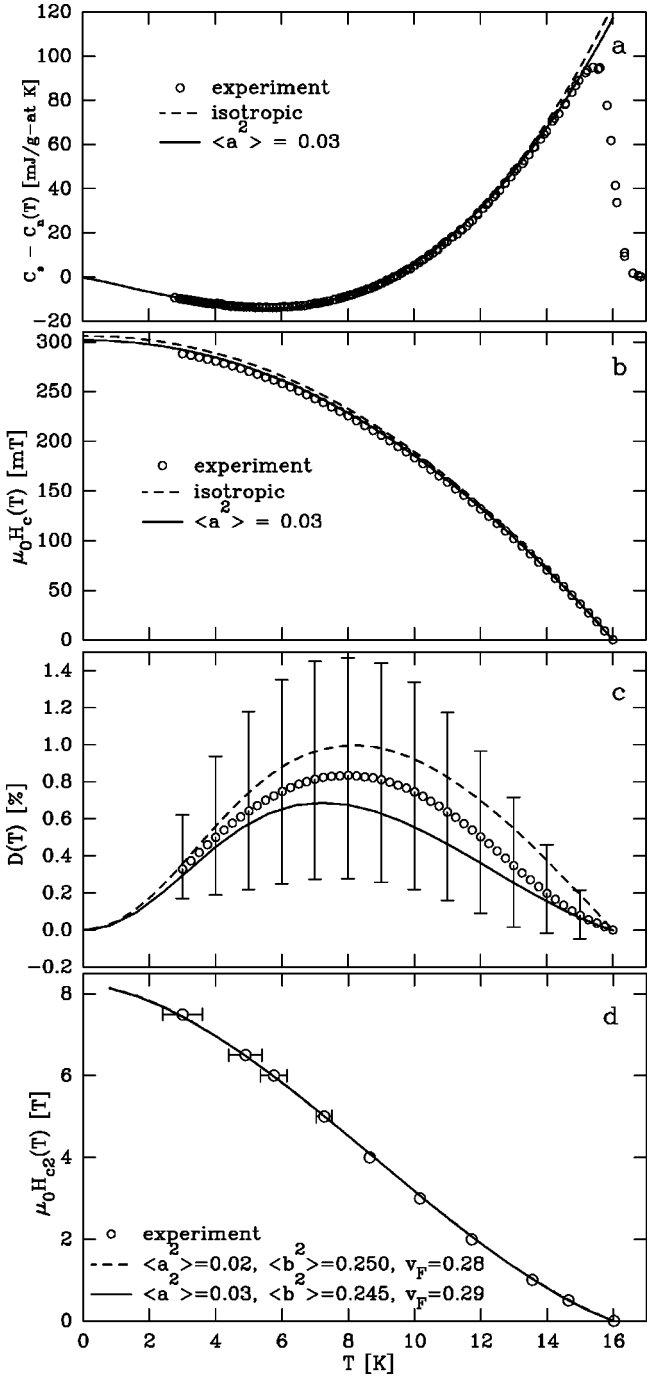

FIG. 8. Specific heat difference $\Delta C(T)=C_s(T)-C_n(T)$ (a), thermodynamic critical field $H_c(T)$ (b), and deviation function $D(T)$ (c) of $LuNi_2B_2C$ compared to theoretical calculations for an isotropic and an anisotropic case with $\langle a_{\mathbf{k}}^2\rangle=0.03$. The upper critical field (d) is a fit to the experiment with anisotropy parameters $\langle a_{\mathbf{k}}^2\rangle=0.02$ and 0.03.

$$D(T)=\frac{H_c(T)}{H_c(0)}-\left[1-\left(\frac{T}{T_c}\right)^2\right]. \tag{10}$$

Error bars of the experimental deviation function result from experimental error bars of the specific heat data and primarily from the extrapolation of $H_c(T)$ to $T\rightarrow 0$. Anisotropy

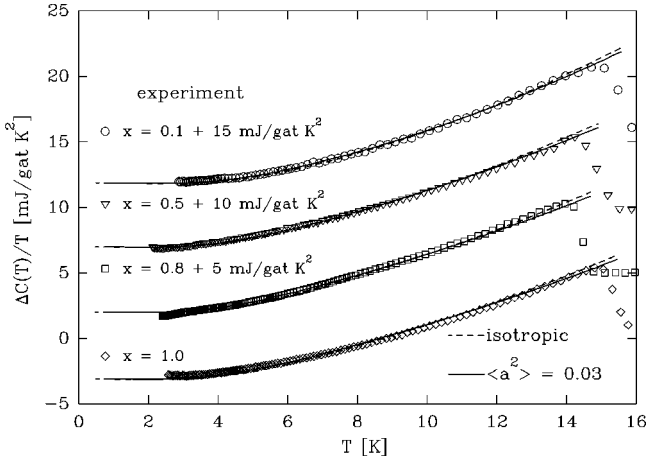

FIG. 9. Specific heat difference $\Delta C(T)=C_s(T)-C_n(T)$, of $Y_xLu_{1-x}Ni_2B_2C$ with $x=0.1$, 0.5, 0.8, and 1 compared to theoretical calculations for an isotropic and an anisotropic case with $\langle a_{\mathbf{k}}^2\rangle=0.03$.

effects push the deviation function towards the weak coupling regime as shown in Fig. 8(c). Even with the large error bar attached to the experimental data, it becomes obvious that the BCS result is far off with its minimum at about -3.7%.

The upper critical field $H_{c2}(T)$ was fit to the experimental data by describing the positive curvature at T_c with the Fermi velocity anisotropy parameter $\langle b_{\mathbf{k}}^2\rangle$ at a fixed mean Fermi velocity $\langle v_F\rangle$, and by changing the anisotropy parameter $\langle a_{\mathbf{k}}^2\rangle$ of the electron phonon coupling strength to de-

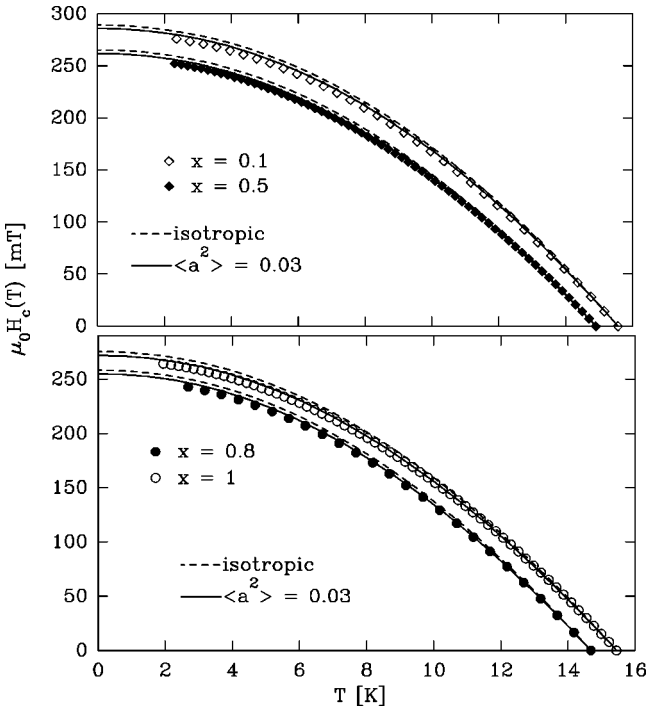

FIG. 10. Thermodynamic critical field $H_c(T)$ for the samples with $x=0.1$, 0.5, 0.8, and 1 compared to theoretical calculations for an isotropic and an anisotropic case with $\langle a_{\mathbf{k}}^2\rangle=0.03$.

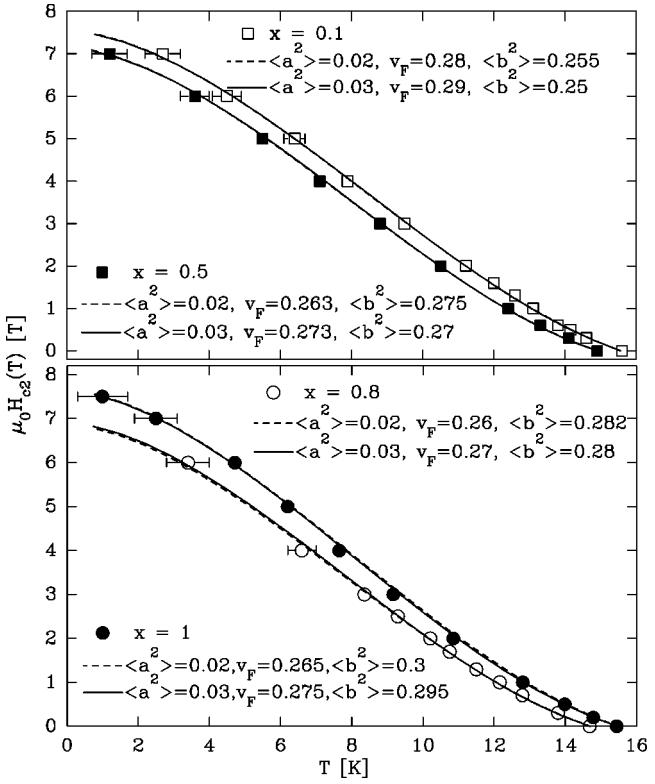

FIG. 11. Upper critical field H_{c2} of $Y_xLu_{1-x}Ni_2B_2C$ with $x=0.1$, 0.5, 0.8, and 1 compared to theoretical calculations for anisotropic cases with $\langle a_{\mathbf{k}}^2\rangle=0.02$ and 0.03.

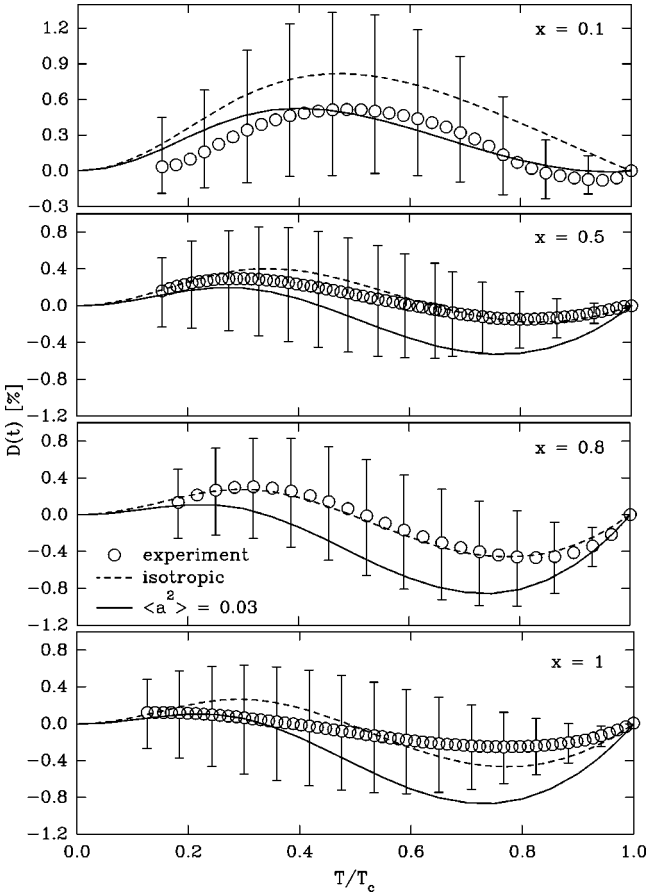

FIG. 12. Deviation function $D(T/T_c)$ of $Y_xLu_{1-x}Ni_2B_2C$ with $x=0.1$, 0.5, 0.8, and 1 compared to theoretical calculations for an isotropic and an anisotropic case with $\langle a_{\mathbf{k}}^2\rangle=0.03$.

scribe the behavior of the experimental curve at lower temperatures. The value of $\langle v_F\rangle$ was taken from the experimental result for the plasma frequency $\hbar\omega_{\mathrm{pl}}=\sqrt{4\pi e^2 v_F^2 N(0)/3}=4.0$ eV (see Ref. 18) which results in a mean Fermi velocity $\langle v_F\rangle$ of $\simeq 0.28\times 10^6$ m/s for $LuNi_2B_2C$.[6] A reasonable fit of the experimental data with this value is achieved with $\langle a_{\mathbf{k}}^2\rangle=0.02$ and $\langle b_{\mathbf{k}}^2\rangle=0.25$. According to the thermodynamic properties, it would as well be possible to apply a higher anisotropy parameter, i.e., $\langle a_{\mathbf{k}}^2\rangle=0.03$. Error bars of the plasma frequency were not given in Ref. 18, and a change of 0.01×10^6 m/s in $\langle v_F\rangle$ is likely to be within the experimental error range. For an anisotropy parameter of $\langle a_{\mathbf{k}}^2\rangle=0.03$, one has to reduce $\langle b_{\mathbf{k}}^2\rangle$ and enhance $\langle v_F\rangle$ to compensate the change as depicted in the bottom frame of Fig. 8. The error bars of the experimental upper critical field result from the width of the transition in the resistivity data.

Figures 9, 10, 11, and 12 show the results for the samples with $x=0.1$, 0.5, 0.8, and 1. Thermodynamic properties and H_{c2} of the whole series can be described with anisotropy parameters $\langle a_{\mathbf{k}}^2\rangle$ between 0.02 and 0.03, which is relatively small compared to the Fermi velocity anisotropy $\langle b_{\mathbf{k}}^2\rangle$ ranging from 0.245 to 0.3 and is comparable to the electron-phonon anisotropy parameters of $LaAl_2$ (Ref. 25, $\langle a_{\mathbf{k}}^2\rangle=0.01$), Nb (Ref. 14, $\langle a_{\mathbf{k}}^2\rangle=0.0335$) and is smaller than the anisotropy parameter of Nb_3Sn (Ref. 26, $\langle a_{\mathbf{k}}^2\rangle=0.08$). The Fermi velocity anisotropy parameters of $Y_xLu_{1-x}Ni_2B_2C$ are obviously higher than those of $LaAl_2$ ($\langle b_{\mathbf{k}}^2\rangle=0.16$), Nb ($\langle b_{\mathbf{k}}^2\rangle=0.118$), and Nb_3Sn ($\langle b_{\mathbf{k}}^2\rangle=0.13$). In comparing the upper critical field of YNi_2B_2C to that of $Y_{0.5}Lu_{0.5}Ni_2B_2C$ it is obvious that the positive curvature of H_{c2} at T_c is rather pronounced in both samples. If the T_c reduction had been caused by impurity scattering the positive curvature of H_{c2} at T_c would have been gradually reduced with increasing impurity concentration as was demonstrated by Weber *et al.*[14] in their analysis of polycrystalline Nb. Such an effect can certainly not be observed in our case.

D. T_c reduction in the series $Y_xLu_{1-x}Ni_2B_2C$

The reduction of T_c within the series cannot be described with impurity scattering in terms of Eliashberg theory because this would require randomly distributed scattering centers. A substitution of Lu with Y or vice versa produces inhomogeneities of the periodic potential only on the rare earth lattice site, so that a random distribution can only be expected with small substitutions up to $x=0.1$. If the T_c reduction should be explained by inelastic impurity scattering expressed by the scattering rate t^+, it is restricted to the condition that the electronic properties of the system, as, e.g., $N(0)$, remain unchanged, which is not the case in $Y_xLu_{1-x}Ni_2B_2C$ (see Fig. 13). Thus, the T_c-reduction within the series cannot be attributed to inelastic impurity scattering expressed by t^+.

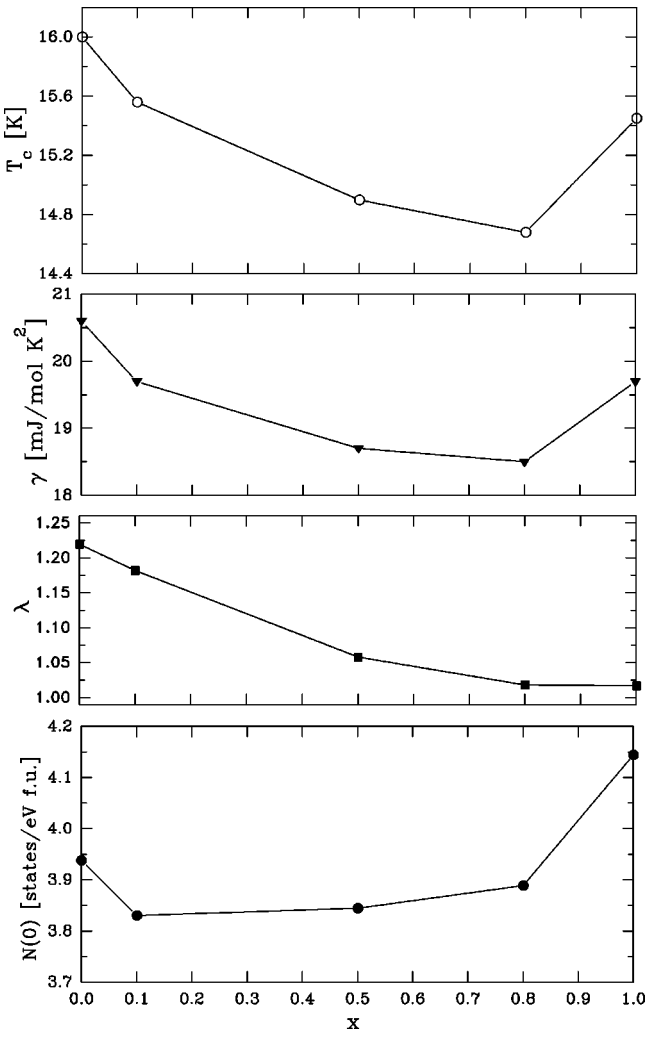

FIG. 13. The critical temperature T_c, electron-phonon coupling strength λ, Sommerfeld constant γ, and density of states $N(0)$ as a function of x for the series $Y_xLu_{1-x}Ni_2B_2C$.

The density of states $N(0)$ (Fig. 13) was calculated using the bare Sommerfeld constant $\gamma^*=\gamma/(1+\lambda)$ and the number of atoms per cm^3 n_A in the approximation $N(0)\propto n_A\gamma^*$. Unlike the electron-phonon coupling factor λ, γ behaves as T_c as a function of x, therefore accounting for a similar behavior of $N(0)$. Hence, as λ decreases with decreasing Lu content, $N(0)$ shows a minimum between $x=0$ and 1. Obviously, the behavior of T_c results from an interplay of the coupling strength of electrons to phonons and the density of states at the Fermi level. The latter is most likely due to a band broadening arising from the *R*-ion size mismatch which washes out the maximum of the electronic density of states at the Fermi energy. The $N(0)$ values of the unalloyed compounds YNi_2B_2C (4.14 states/eV f.u.) and $LuNi_2B_2C$ (3.94 states/eV f.u.) agree closely with the values of 4.31 and 4.06 states/eV f.u., respectively, reported by Divis *et al.*[27] from calculations based on the density functional theory.

E. Thermodynamics and H_{c2} of $La_3Ni_2B_2N_{3-\delta}$

The model spectrum of $La_3Ni_2B_2N_{3-\delta}$ (Fig. 14) was obtained in a similar manner as the spectra of the borocarbides (Ref. 20) and is cut off at the local minimum at ~50 meV. After applying a coupling function $\alpha^2(\omega)\sim\omega^s$ with $s=-1/2$, the spectrum was rescaled with a constant factor to give the critical temperature $T_c=11.73$ K and a fixed pseudopotential $\mu^*=0.13$. This results in a coupling strength of $\lambda=1.02$. With the Sommerfeld constant $\gamma=24$ mJ/mol K^2, the thermodynamic properties were calculated for an isotropic and an anisotropic clean limit case with $\langle a_{\mathbf{k}}^2\rangle=0.08$ (Fig. 15). We note, that the clean limit approximation may, of course, be questioned because of the rather high residual resistance reported in Ref. 5 where all data used for the present analysis have been measured on one individual sample. Supposing the high $\rho_0\simeq 9$ $\mu\Omega$ cm to be intrinsic, we had to consider an impurity scattering rate $t^+\simeq 10$ meV which, however, did not allow to find any reasonable set of parameters describing the experimental results on the upper critical field and specific heat. In the view of the present Eliashberg approach, these data are compatible with scattering rates $t^+\leqslant 1$ meV indicating that the high $\rho_0\simeq 9$ $\mu\Omega$ cm of $La_3Ni_2B_2N_{3-\delta}$ arises from scattering on the grain boundaries rather than from an intrinsic scattering inside the grains which were shown by high resolution electron microscopy (HREM) to be practically free of defects on the HREM scale.[5]

The upper critical magnetic field $H_{c2}(T)$ shown in Fig. 15 was fitted with the anisotropy parameter obtained from the analysis of the thermodynamic properties, $\langle a_{\mathbf{k}}^2\rangle=0.08$, a mean Fermi velocity $\langle v_F\rangle=0.225\times 10^6$ m/s and its anisotropy parameter of $\langle b_{\mathbf{k}}^2\rangle=0.245$. A fit to the experimental data with an anisotropy parameter of $\langle a_{\mathbf{k}}^2\rangle=0.06$ is included for comparison. The mean Fermi velocity obtained in the analysis lies between the root mean square anisotropies $\sqrt{\langle v_x^2\rangle}=0.292\times 10^6$ m/s and $\sqrt{\langle v_z^2\rangle}=0.148\times 10^6$ m/s calculated by Singh and Pickett.[3] In contrast to the borocarbides a consistent description of the thermodynamic properties and the upper critical field can also be achieved with $s=0$, which results in an electron-phonon coupling factor $\lambda=0.87$, anisotropy parameters $\langle a_{\mathbf{k}}^2\rangle=0.06$ and $\langle b_{\mathbf{k}}^2\rangle=0.27$, and a mean Fermi velocity of $\langle v_F\rangle=0.2\times 10^6$ m/s. Different coupling factors λ are obtained with different coupling functions $\alpha^2(\omega)\sim\omega^s$ ($s=0,-1/2$) because, after rescaling the spectral functions to obtain the critical temperature of the system and a pseudopotential $\mu^*=0.13$, the low-energy contributions to $\alpha^2F(\omega)$ are enhanced with $s=-1/2$ compared to the case of $s=0$. The coupling factor λ obtained with the coupling function $\alpha^2(\omega)\sim\omega^0$ is in good agreement with the estimate $\lambda\equiv\gamma/\gamma_{bs}-1=0.85$. In general, both descriptions ($s=0$, $-1/2$) require a higher value for the anisotropy parameter $\langle a_{\mathbf{k}}^2\rangle$ compared to the borocarbides in order to describe the experimental data, because the agreement between theory and experiment improves with increasing $\langle a_{\mathbf{k}}^2\rangle$ as is clearly demonstrated by the comparison with the specific-heat difference, the thermodynamic critical field, and the deviation function of $La_3Ni_2B_2N_{3-\delta}$ shown in Fig. 15. The rather large anisotropy of $\langle a_{\mathbf{k}}^2\rangle\simeq 0.08$ further explains the temperature dependence of the upper critical field and $H_{c2}(0)$ of ~8 T comparable to that of $LuNi_2B_2C$, since $\langle a_{\mathbf{k}}^2\rangle$ has an enhancing effect on H_{c2}.

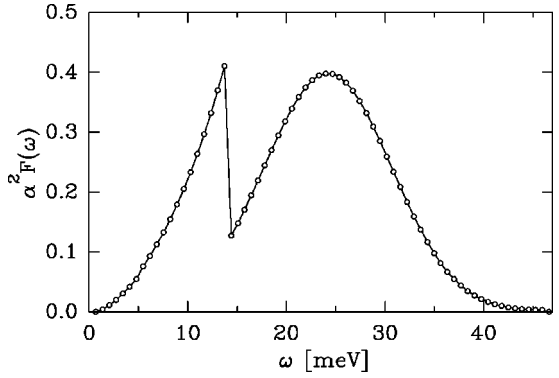

FIG. 14. Spectral density $\alpha^2F(\omega)$ used in the analysis of $La_3Ni_2B_2N_{3-\delta}$ obtained from a model phonon spectrum, which was rescaled to give the critical temperature of the sample $T_c = 11.73$ K and for a fixed pseudopotential $\mu^* = 0.13$.

F. Comparison of $Y_xLu_{1-x}Ni_2B_2C$ and $La_3Ni_2B_2N_{3-\delta}$

The most distinctive feature of the borocarbide and boronitride superconductors pointed out in previous papers[5,28] is the temperature dependence of the electronic specific heat in the superconducting state: While Y and $LuNi_2B_2C$ exhibit an almost cubic temperature dependence of $C_{eS}(T)$, $La_3Ni_2B_2N_{3-\delta}$ shows an approximately exponential behavior of $C_{eS}(T)$ close to the BCS predictions. Thus, $La_3Ni_2B_2N_{3-\delta}$ was supposed to be a weak-coupling BCS superconductor, because other characteristics of the superconducting state of the boronitride such as the thermodynamic ratios (e.g., $\Delta C/\gamma T_c = 1.4$) and the deviation function $D(t)$ (see Fig. 16) were also found to be much closer to the BCS predictions than those of the borocarbides. The above analysis of the thermodynamic properties and the upper critical field, however, demonstrates that the difference between the thermodynamic ratios and the deviation function of the borocarbides and the boronitride arises from a larger anisotropy of the electron-phonon interaction in the latter rather than from a smaller coupling strength ($\lambda \simeq 0.87$ or 1.02 for $La_3Ni_2B_2N_{3-\delta}$ compared to $\lambda \simeq 1.02-1.22$ for $Y_xLu_{1-x}Ni_2B_2C$). The different temperature dependence of the heat capacity in the superconducting state—cubic in case of the borocarbides—cannot be explained by our Eliashberg calculations which fit the specific heat difference $\Delta C = C_s - C_n$, but not the absolute $C_{eS}(T)$, of, e.g., YNi_2B_2C depicted in Fig. 17 as a semilogarithmic plot of $C_{eS}/\gamma T_c$ versus the inverse reduced temperature T_c/T. As the gap obtained by the above calculations is free of nodes, it yields an exponential temperature dependence for $C_{eS}(T)$ which becomes linear in the semilogarithmic representation. This is in contrast to the experimental result for YNi_2B_2C which exhibits a pronounced curvature in this plot indicative for a power law. In Sec. IV C we noted, that a satisfactory description of the thermodynamic properties of the borocarbides and in particular their thermodynamic critical field is only achieved when the calculations are performed with gamma values of about 5% smaller than the experimental values. By adding a linear contribution corresponding to the 5% of the normal state gamma value (1.1 mJ/mol K^2) omitted before, an improvement of the temperature dependence of the calculated $C_{eS}(T)$ is achieved (dashed line in Fig. 17). These ad-

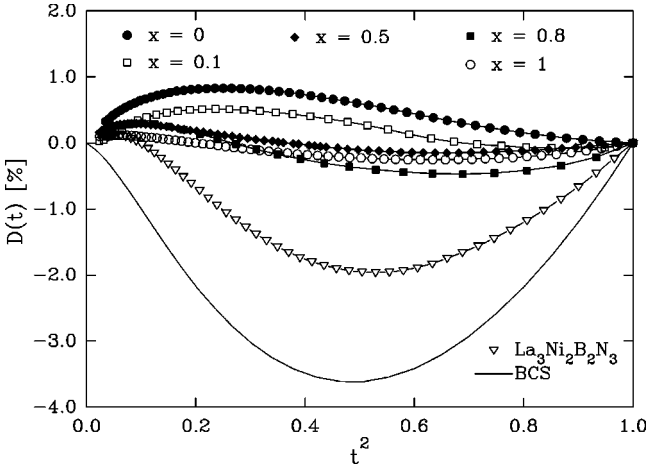

FIG. 16. Deviation functions $D(T/T_c) = D(t)$ vs t^2 of $Y_xLu_{1-x}Ni_2B_2C$ and $La_3Ni_2B_2N_{3-\delta}$. The BCS result (solid line) was added for comparison.

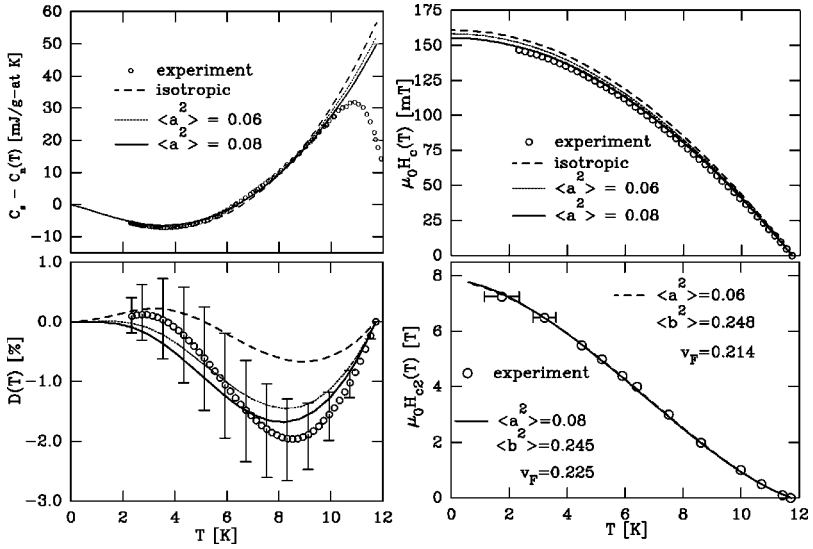

FIG. 15. Specific heat difference $\Delta C(T) = C_s(T) - C_n(T)$, thermodynamic critical field $H_c(T)$, and magnetic deviation function $D(T)$ of $La_3Ni_2B_2N_{3-\delta}$ compared to theoretical calculations for an isotropic and an anisotropic case with $\langle a_k^2 \rangle = 0.08$. The upper critical field is a fit to the experiment with anisotropy parameters $\langle a_k^2 \rangle = 0.06$ and 0.08.

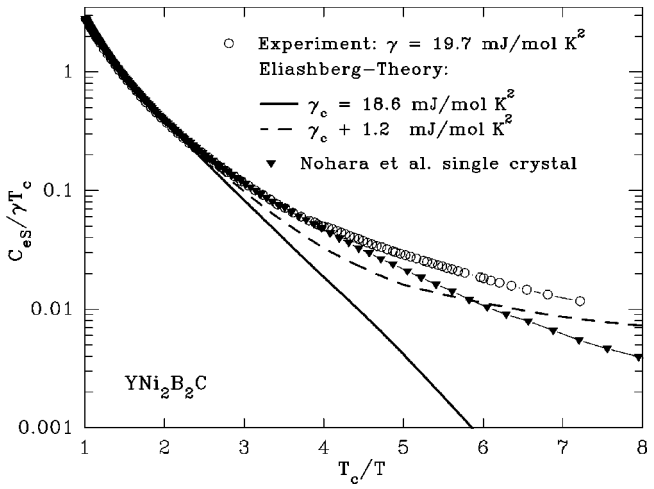

FIG. 17. Electronic specific heat in the superconducting state $C_{es}(T)/\gamma T_c$ vs the inverse reduced temperature T_c/T in a semilogarithmic plot. The solid line was calculated by adding the normal state contribution $\gamma_c T$ to the specific-heat difference between the superconducting and normal state ΔC obtained from the Eliashberg-equations. The data of Nohara *et al.*[10] are labeled by filled triangles.

ditional electronic contributions may be attributed to a normal state impurity phase and/or to contributions from the small electron pocket, for which Terashima *et al.*[24] proposed a significantly reduced gap. The latter argument is supported by the specific heat results obtained on a single crystal YNi_2B_2C by Nohara *et al.*[10] which are included in Fig. 17 for comparison. For temperatures T_c/T between 1 and 5 (i.e., $T=15.5-3$ K) both experimental data sets are in rather good agreement, but clearly deviating from our calculations. Below about 3 K an exponential temperature dependence can be resolved from the data of Nohara *et al.*[10] This may be attributed to the small gap on the electron pocket which can be identified as the third Fermi surface sheet detected by Dugdale *et al.*[7,24] The third Fermi surface sheet was not considered in our calculations because its contribution appeared to be negligible in C_s-C_n. The exponential low-temperature behavior of C_{eS} in particular for the polycrystalline YNi_2B_2C is covered by a linear electronic contribution from small amounts of a secondary phase of about 0.4(2) mJ/mol K^2. Although this contribution is significantly reduced in the samples of the pseudoquaternary system, the overall feature of the semilogarithmic plot is preserved. Accordingly the conclusions concerning the reduced gap on the third Fermi surface sheet can also be drawn for $Y_xLu_{1-x}Ni_2B_2C$.

V. CONCLUSIONS

Model phonon spectra obtained from specific heat measurements, rescaled to give the critical temperatures of the system and for a Coulomb-pseudopotential value of $\mu^*=0.13$, resulted in coupling strengths λ ranging from 1.02 for YNi_2B_2C to 1.22 for $LuNi_2B_2C$. We were able to show that a consistent description of the thermodynamic properties and the upper critical field of the series $Y_xLu_{1-x}Ni_2B_2C$ and the boronitride $La_3Ni_2B_2N_{3-\delta}$ within the Eliashberg theory is achieved only, if anisotropy effects of the electron-phonon coupling and of the Fermi velocity are included. Excellent agreement between theory and experiment was achieved in the analysis of the series $Y_xLu_{1-x}Ni_2B_2C$ with anisotropy parameters $\langle a_{\mathbf{k}}^2\rangle=0.02-0.03$ and $\langle b_{\mathbf{k}}^2\rangle=0.245-0.3$. The model spectral functions for $La_3Ni_2B_2N_{3-\delta}$ yielded coupling factors $\lambda=1.02$ ($s=-1/2$) and $\lambda=0.87$ ($s=0$) comparable to those of $Y_xLu_{1-x}Ni_2B_2C$. The thermodynamic properties and the upper critical field are well described with $\langle a_{\mathbf{k}}^2\rangle=0.08$ and $\langle b_{\mathbf{k}}^2\rangle=0.245$ ($s=-1/2$) or $\langle a_{\mathbf{k}}^2\rangle=0.06$ and $\langle b_{\mathbf{k}}^2\rangle=0.27$ ($s=0$). For $La_3Ni_2B_2N_{3-\delta}$ it is of importance to include anisotropy in order to describe its upper critical field and—in contrast to the borocarbides—its thermodynamic properties.

Coupling and impurity effects are not capable of explaining the T_c behavior within the series $Y_xLu_{1-x}Ni_2B_2C$. The behavior of γ as a function of x suggests $N(0)$, aside from λ, to be the reason for the minimum in $T_c(x)$, which is confirmed by an approximate calculation of $N(0)$ from γ. The approximately cubic temperature dependence of $C_{eS}(T)$ of the borocarbides cannot be accounted for by the current Eliashberg calculations due to a small gap of the third Fermi surface sheet. This contribution, however, is suppressed in ΔC and therefore the Eliashberg calculations are in good agreement with the related experimental thermodynamic properties.

ACKNOWLEDGMENTS

We thank M. Nohara for providing the specific heat data included in Fig. 17. This work was supported by the Austrian Science Foundation under Grant No. P 11090 and by the Kärntner Elektrizitätsgesellschaft (KELAG).

[1] T. Siegrist, H. W. Zandbergen, R. J. Cava, J. J. Krajewski, and W. F. Peck, Jr., Nature (London) **367**, 254 (1994); T. Siegrist, R. J. Cava, J. J. Krajewski, and W. F. Peck, Jr., J. Alloys Compd. **216**, 135 (1994).

[2] L. F. Mattheiss, Phys. Rev. B **49**, 13 279 (1994).

[3] D. Singh and W. Pickett, Phys. Rev. B **51**, 8668 (1995).

[4] H. Michor, G. Hilscher, R. Krendelsberger, P. Rogl, and F. Bourée, Phys. Rev. B **58**, 15 045 (1998).

[5] H. Michor, R. Krendelsberger, G. Hilscher, E. Bauer, C. Dusek, R. Hauser, L. Naber, D. Werner, P. Rogl, and H. W. Zandbergen, Phys. Rev. B **54**, 9408 (1996).

[6] S. V. Shulga, S.-L. Drechsler, G. Fuchs, K.-H. Müller, K. Winzer, M. Heinecke, and K. Krug, Phys. Rev. Lett. **80**, 1730 (1998).

[7] S. B. Dugdale, M. A. Alam, I. Wilkinson, R. J. Hughes, I. R. Fischer, P. C. Canfield, T. Jarlborg, and G. Santi, Phys. Rev. Lett. **83**, 4824 (1999).

[8] J. Freudenberger, S.-L. Drechsler, G. Fuchs, A. Kreyssig, K. Nenkov, S. V. Shulga, K.-H. Müller, and L. Schulz, Physica C **306**, 1 (1998).

[9] K. D. D. Rathnayaka, A. K. Bhatnagar, A. Parasiris, D. G.

Naugle, P. C. Canfield, and B. K. Cho, Phys. Rev. B **55**, 8506 (1997).
[10] M. Nohara, M. Isshiki, F. Sakai, and H. Takagi, J. Phys. Soc. Jpn. **68**, 1078 (1999).
[11] J. M. Daams and J. P. Carbotte, J. Low Temp. Phys. **43**, 263 (1981).
[12] D. Markovitz and L. P. Kadanoff, Phys. Rev. **131**, 563 (1963).
[13] M. Prohammer and E. Schachinger, Phys. Rev. B **36**, 8353 (1987).
[14] H. W. Weber, E. Seidl, C. Laa, E. Schachinger, M. Prohammer, A. Junod, and D. Eckert, Phys. Rev. B **44**, 7585 (1991).
[15] L. Niel, N. Giesinger, H. W. Weber, and E. Schachinger, Phys. Rev. B **32**, 2976 (1985).
[16] P. B. Allen, Phys. Rev. B **13**, 1416 (1976).
[17] J. M. Daams, Ph.D. thesis, McMaster University, Ontario, 1977 (unpublished).
[18] F. Bommeli, L. Degiorgi, P. Wachter, B. K. Cho, P. C. Canfield, R. Chau, and M. B. Maple, Phys. Rev. Lett. **78**, 547 (1997).
[19] V. Ambegaokar, in *Superconductivity*, edited by R. D. Parks (Dekker, New York, 1969), pp. 259.
[20] H. Michor, T. Holubar, C. Dusek, and G. Hilscher, Phys. Rev. B **54**, 9408 (1996).
[21] H. Schmidt and H.F. Braun, in *Studies of High Temperature Superconductors*, edited by A. V. Narlikar (Nova Science Publishers, New York, 1998), Vol. 26, p. 47.
[22] F. Gompf, W. Reichardt, H. Schober, B. Renker, and M. Buchgeister, Phys. Rev. B **55**, 9058 (1997).
[23] A. Junod, T. Jarlborg, and J. Muller, Phys. Rev. B **27**, 1568 (1983).
[24] T. Terashima, C. Haworth, H. Takeya, S. Uji, H. Aoki, and K. Kadowaki, Phys. Rev. B **56**, 5120 (1997).
[25] B. Vlcek, E. Seidl, W. Weber, E. Schachinger, and W. Pint, Physica C **167**, 198 (1990).
[26] E. Schachinger and M. Prohammer, Physica C **156**, 701 (1988).
[27] M. Divis, K. Schwarz, P. Blaha, G. Hilscher, H. Michor, and S. Khmelevsky, Phys. Rev. B **62**, 6774 (2000).
[28] G. Hilscher and H. Michor, in *Studies of High Temperature Superconductors*, edited by A. V. Narlikar (Nova Science Publishers, New York, 1999), Vol. 28, p. 241.